Journal of Pressure Vessel Technology, Vol. 131, 2009, 041401

The Effects of Filler Metal Transformation Temperature on Residual Stresses in a High Strength Steel Weld

J. A. Francis
School of Materials
University of Manchester,
Grosvenor Street, Manchester M1 7HS, U.K.

H. J. Stone
Materials Science and Metallurgy
University of Cambridge,
Pembroke Street, Cambridge CB2 3QZ, U.K.

S. Kundu
Materials Science and Metallurgy
University of Cambridge,
Pembroke Street, Cambridge CB2 3QZ, U.K.

R. B. Rogge
Canadian Neutron Beam Centre
National Research Council, Canada
Chalk River Laboratories,
Chalk River, Ontario KOJ 1PO, Canada

H. K. D. H. Bhadeshia
Materials Science and Metallurgy
University of Cambridge,
Pembroke Street, Cambridge CB2 3QZ, U.K.

P. J. Withers
School of Materials
University of Manchester,
Grosvenor Street, Manchester M1 7HS, U.K.

L. Karlsson
ESAB AB, Central Research Laboratories
Lindholmsallén 9, P.O. Box 8004,
SE-402 77 Gothenburg, Sweden

ABSTRACT

Residual stress in the vicinity of a weld can have a large influence on structural integrity. Here the extent to which the martensite-start temperature of the weld filler metal can be adjusted to engineer the residual stress distribution in a bainitic-martensitic steel weld has been investigated. Three single-pass groove welds were deposited by manual-metal-arc welding on 12 mm thick steel plates using filler metals designed to have different martensite-start temperatures. Their longitudinal, transverse and normal residual stress distributions were then characterised across the weld cross-section by neutron diffraction. It was found that tensile stresses along the welding direction can be reduced or even replaced with compressive stresses if the transformation temperature is lowered sufficiently. The results are interpreted in the context of designing better welding consumables.

Keywords: bainite, martensite, neutron diffraction, phase transformation, transformation strain, weld metal.

INTRODUCTION

In assessing the integrity of an engineering structure it is necessary to estimate both the external or primary loads acting on critical components, as well as any secondary loading associated with residual stresses. The latter can have significant effects on the susceptibility of a material to degradation mechanisms such as fatigue and environmentally-assisted cracking. Residual stresses arise as a result of welding operations because they involve the deposition of molten filler metal and the localised input of intense heat. In the case of steels, the problem can be complicated by the fact that various solid-state phase transformations can occur during cooling of the material. For example, in a given steel, low cooling rates might lead to the formation of ferrite and pearlite via a diffusional phase transformation. On the other hand, more rapid cooling might induce martensite formed by a shear transformation. Indeed, the significantly different displacements associated with these phase changes can have dramatically different consequences for the development of residual stress in the system as a whole [1-4].

The conventional way of coping with the prospect of high weld residual stresses is to reduce design stresses, or to conduct post weld heat treatments to relieve the residual stresses. The former leads to underperformance while the latter is not always logistically possible. An alternative approach for steels exploits displacive phase transformations to control the development of residual stresses. This is the focus of the current paper.

When austenite in steels transforms into plates of bainite or martensite, the phase change causes a deformation which is an invariant-plane strain consisting of a large shear on the habit plane and a dilatational strain normal to the plane. Each austenite grain can transform into 24 different crystallographic variants of the plates. If each variant occurs in equal measure the shears cancel so that the macroscopic shape deformation simply reflects the volume change. However, external stress can favour the formation of specific variants. This selectivity may counteract the build up of tensile stresses arising from the contraction of the weld as it cools. If, however, the transformation exhausts before cooling is complete then further contraction can lead once again to the build up of stresses until ambient temperature is achieved.

It is important therefore to tailor the transformation temperature of the filler alloy through judicious alloying such that the compensation process can be sustained to ambient temperature. In this way Ohta *et al*. [5, 6] and Wang *et al*. [7] were able to realize transformation induced stress-relief, and demonstrated a significant increase in the fatigue crack propagation resistance of weldments. In the present work weld filler materials have been designed with this stress compensating mechanism in mind but which are also tough, with the aim of improving performance in actual welded joints.

EXPERIMENTAL DETAILS

Filler Metals

Three filler alloy compositions were chosen in the current study. The filler alloy, OK75.78, is a commercially available electrode for which transformation should exhaust before ambient temperature is reached [8]. LTTE is a filler that was proposed by Wang *et al*. [7], with a low martensite-start (M_S) temperature, and it has been shown to achieve improved fatigue performance in welded joints. Finally, the filler designated "Series B" is an alternative formulation selected by the current authors. The intention here was to improve on the solidification behaviour and toughness exhibited by LTTE, while still achieving a similar M_s temperature. The compositions are summarised in Table 1.

Table 1: Approximate compositions of base plate and undiluted filler alloys in wt. %.

Material	C	Si	Mn	Cr	Ni	Mo	Cu
Weldox 960	0.20	0.50	1.6	0.7	2.0	0.7	0.3
OK 75.78	0.05	0.19	2.0	0.4	3.1	0.6	-
LTTE	0.07	0.20	1.3	9.1	8.5	-	-
Series B	0.03	0.65	0.5	1.0	12.0	0.5	-

The bainite-start (B_S) and M_S temperatures for bainitic-martensitic filler alloys can be estimated using a computer program developed as part of the Materials Algorithm Project [9]. Details of the underlying principles for the software are available in the literature [10-12]. The B_S and M_S temperatures were estimated in this way for each of the undiluted filler alloys and they are summarised in Table 2. While it was possible to calculate B_S temperatures for both the LTTE and Series B filler metals, in both cases they fell below the corresponding M_S temperature; in other words bainite does not occur in these alloys as they are martensitic. Note also that the shape deformations arising due to the formation of bainite and martensite are essentially the same so for the present purposes it is only important to focus on the transformation temperatures [13].

Table 2: Estimates for B_S (if applicable) and M_S (ºC) for base plate and undiluted filler alloys.

Parameter	Base Plate	OK75.78	LTTE	Series B
B_S	460	410	--	--
M_S	370	400	280	250

As expected, both LTTE and Series B have transformation temperatures that are significantly lower than those for OK75.78. Note that the martensite start temperature is determined by the point where the free energy change for the diffusionless transformation of austenite reaches a critical value, and that the free energy change in turn depends on the solutes present. It should not, therefore, be surprising to see two alloys with markedly different compositions having similar start temperatures [14]. Finally, typical mechanical properties are given, where possible, for each of the alloys used in this study, in Table 3 [15-17].

Table 3: Summary of available mechanical properties for base plate and undiluted filler alloys [15-17].

Alloy	Yield (MPa)	UTS (MPa)	Elongation (%)	Charpy Energy (J)			
				-60 °C	-40 °C	-20 °C	+20 °C
Weldox 960	> 960	980 - 1150	>12	-	27	27-30	-
OK75.78	~ 1000*	-	-	65	79	90	96
LTTE	1135	1287	6	15	17	15	20
Series B	~ 1100*	-	-	28	22	27	28

* Estimate based on Vickers hardness.

Satoh Tests on Filler Metals

Satoh tests [18, 19] were carried out to characterise the mechanical response of each undiluted filler alloy during cooling from the austenitic state. To do this, an unconstrained matchstick-shaped sample was austenitized by heating to 850 °C for 60 s; it was then rigidly constrained at its ends and allowed to cool at 10 °C s^{-1} under this restraint whilst monitoring the stress.

Manufacture of Welded Plates

Three identical plates ($375 \times 200 \times 12\ mm^3$) were prepared from the high strength bainitic-martensitic steel, Weldox 960. Along the center of each plate, a 5 mm deep Vee-groove was machined with an included angle of 60 °. Some manual grinding then took place so that, in each case, the final groove geometry included a radius of approximately 2.5 mm at the root and an opening of approximately 6 mm at the plate surface. The filler metals used were those listed in Table 1. Welding was undertaken in the down-hand position. Initially, it was intended to use a heat input for each weld in the range between 1.1 and 1.4 kJ mm^{-1}, as has been previously reported [20]. However, it was found that larger heat inputs were required to fill the groove adequately in a single pass. As such, the nominal heat inputs ranged between 2.2 and 2.5 kJ/mm, with the preheat temperature being 125 °C and the plates being restrained by clamping during welding in all cases. A visual inspection of the plates after welding revealed that any distortion was minimal.

Stress Measurements in Welded Plates

Neutron diffraction is known to be an effective technique for measuring bulk residual stresses in welds [21]. As such, measurements of the residual stresses in the welded plates were conducted by neutron diffraction on the L3 spectrometer, which is part of the National Research Council of Canada facility at the NRU reactor, Chalk River.

Monochromation of the neutron beam was achieved by diffraction from the $\{\bar{1}\bar{1}5\}$ planes of a germanium monochromator crystal at 92 °. The wavelength of the neutrons was 1.5651 ± 0.0001 Å from calibration measurements of the first four diffraction peaks using a nickel standard powder sample. With this wavelength, the {112} peaks from the ferritic and martensitic material in the welded plates could be observed at an angle of $2\theta \approx 84°$ which, being close to 90 °, provided optimal spatial resolution and avoided peak asymmetry arising as a result of axial divergence.

Positioning of the sample in the neutron beam was accomplished with an *XYZ* translation stage attached to a 360 ° rotational drive. With these drives, the sample could be positioned with an accuracy of 0.1 mm in *X, Y* and *Z* and 0.1 ° in rotational angle. Spatial resolution within the sample was achieved by placing cadmium slits in the paths of the incident and diffracted beams. For all of the measurements, the slits were positioned within 20 mm of the sample surface to avoid penumbra effects.

Determination of the full strain tensor at each measurement position requires the measurement of the lattice strain in at least six independent directions. However, it is possible to determine the axial, transverse and normal stresses (irrespective of whether they are principal axes) from the corresponding strains [22]. Whilst it is likely that one of the principal axes lies along the welding direction, the geometry of the weld fusion zone may be expected to lead to rotations of the principal axes from the transverse and normal directions in this plane.

Measurements of the lattice strains were made in the plane perpendicular to the welding direction across the center of each plate (Figure 1). For measurements in the transverse and normal directions, the samples were orientated on the translation stage with the welds vertical. Slits 1 mm wide and 10 mm in the vertical direction were employed, providing a nominal gauge volume of $1 \times 1 \times 10\ \text{mm}^3$ in the sample. This choice of gauge volume presupposes that the strains will be invariant along the welding direction. For the measurement of the longitudinal strains the samples were orientated with the transverse direction vertical and the welds parallel to the scattering vector. For these measurements, slits 1 mm wide and 2 mm in the vertical direction were used. For all strain measurements, data acquisition times were chosen to ensure that an associated error in strain of less than 100 microstrain was achieved.

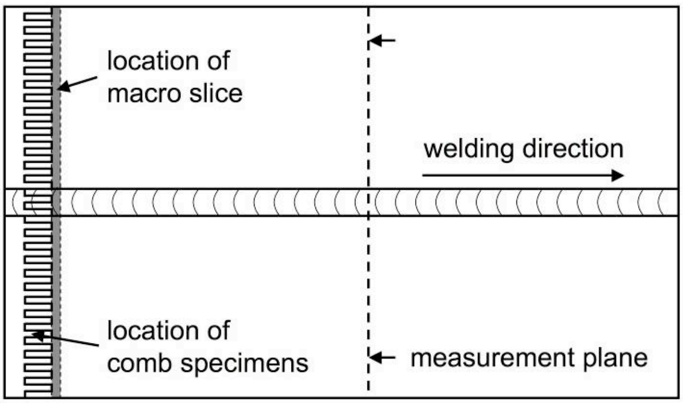

Figure 1: Schematic representation of welded plate showing location of reference combs, slice extracted for macrograph and location of measurement plane.

Determination of Strain-Free (d_0) Lattice Spacings

To eliminate the effects of compositional variations on the lattice spacings, stress-free samples were cut from the weld so that reference (d_0) lattice parameters could be measured [23]. The samples were cut by electro-discharge machining from the last 30 mm of each welded plate, as a series of combs, with teeth 2 mm by 2 mm in section and 20 mm long (Figure 1). The dimensions of the teeth were chosen to allow the diffraction gauge volume to be fully immersed in the sample. The long direction of the teeth was aligned parallel with the welding direction in order to avoid stress gradients along them prior to machining. This ensured that minimal macro stresses were retained within the teeth. This also provided maximum spatial resolution for lattice parameter variations in the transverse plane. Combs were extracted from each plate at depths of 1, 3.5, 6, 8.5 and 11 mm from the top surface of the plate.

Metallography

Macrographs were prepared so that the measured residual stress distributions could be correlated with the different metallurgical zones across each of the welded plates. One 5 mm thick slice was removed from the end of each plate by electro-discharge machining (Figure 1). Each slice was then ground and polished to a 1 μm finish prior to etching in 2 % Nital for 15 seconds. The resulting macrograph is shown for each weld in Figure 2. It can be seen that the weld bead penetrations are close to 6 mm, equivalent to half the plate thickness. Whilst there are minor variations from one sample to another, the etching patterns would also suggest that the dimensions of both the fusion zone and heat-affected zone (HAZ) in each weld appear to be similar, in accordance with having used the same nominal welding parameters in each case.

The microstructures across each weld were examined to further clarify the extent of the HAZ. In Figure 2, locations “a” through to “e” are marked on the LTTE macrograph, and these positions correspond to the micrographs that are presented in Figures 3a to 3e respectively. The higher magnification images in Figure 3 confirm the location of the fusion zone at position “a” (see Fig. 3a), the coarse-grained HAZ at position “b” (Fig. 3b), the fine-grained HAZ at position “c” (Fig. 3c), the intercritically-annealed or partially-austenitised HAZ at position “d” (Fig. 3d) and finally un-affected base metal at position “e” (Fig. 3e). Indeed, the microstructure within the coarse-grained HAZ (Fig. 3b) reveals many of the features of a bainitic-martensitic steel, showing evidence of preserved austenite grain boundaries and plate-like structures within the prior-austenite grains. Here, the dark-etching regions are indicative of the presence of carbides and thus a bainitic microstructure, whereas the light-etching regions are likely to be martensite. The intercritical HAZ (Fig. 3d) reveals lighter etching regions that are likely to be ferrite (i.e. regions that were not austenitised during welding) as well as both intermediate and dark regions. The darkest regions in Figure 3d will have transformed to austenite during welding and, due to carbon enrichment, may have transformed to a fine pearlitic microstructure on cooling [24]. Perhaps conveniently then, the metallography appears to confirm that the outer boundary of the HAZ corresponds closely with the light-etching band that appears on the macrographs in Figure 2, at the location that is highlighted on the LTTE weld. Of course, adjacent to the intercritical HAZ there will also be a narrow region that has not undergone any transformations during welding, but may still be over-tempered (the tempered zone) [24]. Nevertheless, the demarcation line on the LTTE weld in Figure 2 separates the regions that were influenced by phase transformations from those that were not.

It is important to note that for the weld nuggets the compositions will have deviated from those listed in Table 1 as a consequence of dilution by the parent material. The dilution level was estimated to be 50% from a macrograph through the weld made with OK75.78. With this in mind, weld metal compositions and transformation temperatures were then estimated for each of the diluted weld metals, and these values are summarised in Table 4. It is worth noting that a dilution level of 50 % could be considered to be an upper limit on the level of dilution that might be experienced in practice. For lower levels of dilution, the composition of the weld metal will tend towards the composition of the undiluted filler wire.

Interestingly, in the case of OK75.78, it can be seen that dilution has had the effect of decreasing the B_S temperature while increasing the M_S temperature when compared with the undiluted alloy. This is due to the different effects of carbon on the mechanisms of bainitic and martensitic transformations. The authors expect that the uncertainties in these estimates are likely to be approximately +/- 20 °C. Indeed, this error correlates closely with the error in measuring temperatures in homogeneous steels. Nevertheless it can be seen that, even at high levels of dilution, both of the low-M_s weld metals still transform at a significantly lower temperature than for the OK75.78 weld metal, so the effects of transformation temperature on the residual stress distributions can still be assessed.

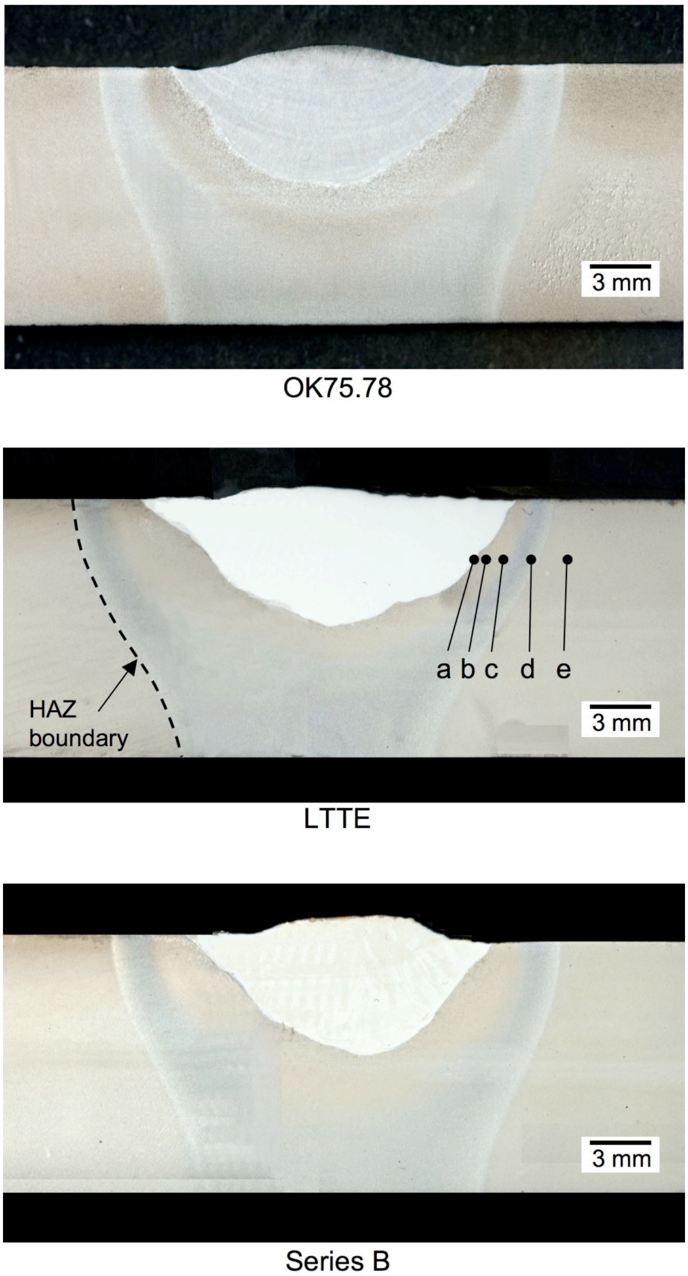

Figure 2: Macrographs through the 12 mm thick welded plates. The extents of the fusion zone and HAZ are similar in each case. The locations at which optical micrographs have been captured (see Figures 3a - 3e) are shown on the LTTE macrograph.

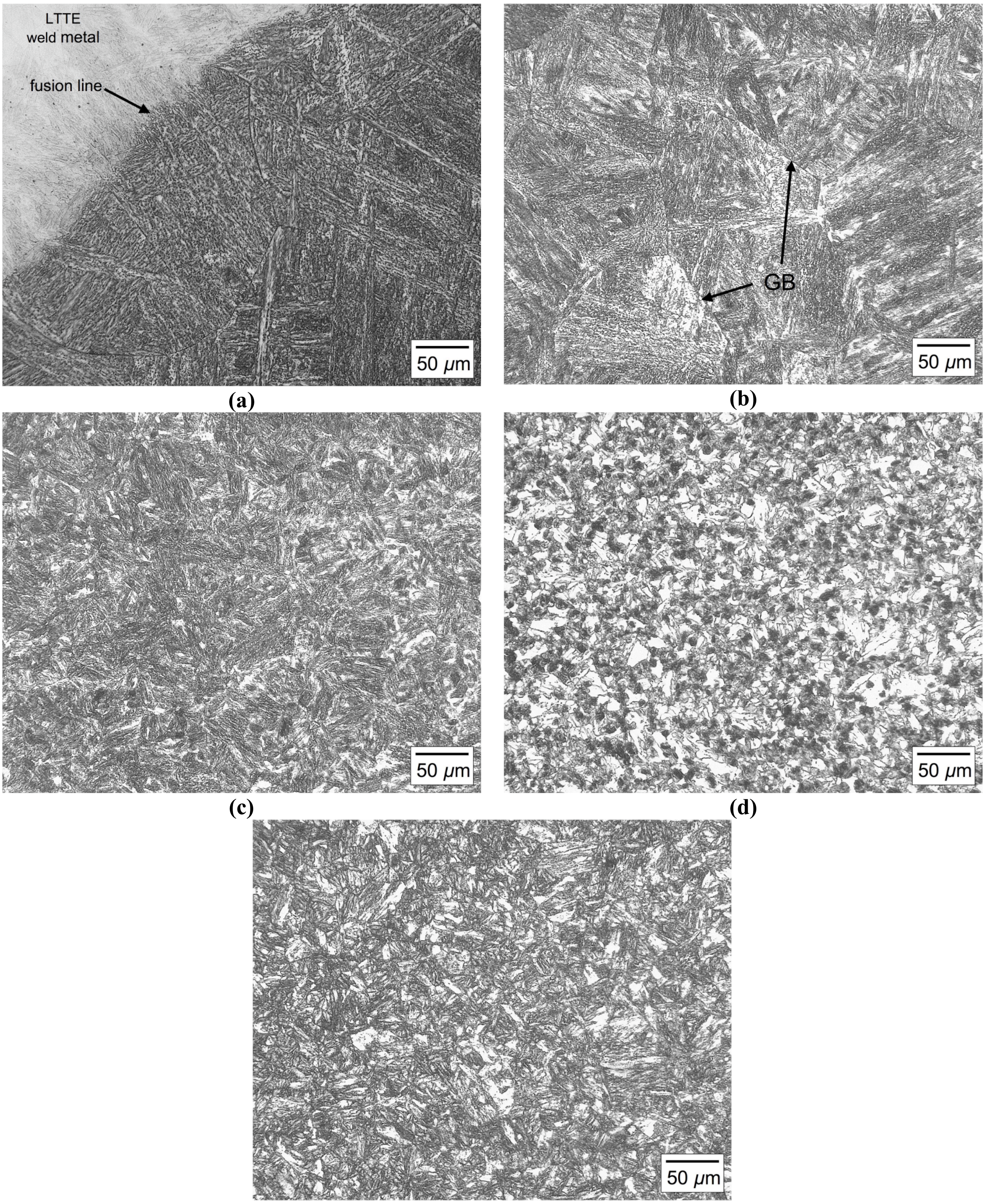

Figure 3: Optical macrographs taken from the LTTE weld at the locations shown in Figure 2. The images show (a) the fusion boundary; (b) coarse-grained HAZ; (c) fine-grained HAZ; (d) intercritical HAZ; and (e) unaffected base metal. In (b) "GB" denotes prior-austenite grain boundaries.

Table 4: Estimates for B_S (if applicable) and M_S (ºC) for weld metals at 50% dilution.

Parameter	OK75.78	LTTE	Series B
B_s	440	--	--
M_s	390	330	320

ANALYSIS OF RESIDUAL STRESS DATA

The measured 112 diffraction peaks were fitted to a Gaussian function having a constant background. In this manner the Bragg angle, θ_{112}, was determined point by point across the measurement plane within each welded sample. The position-dependent lattice spacings, d_{112}, were then obtained from the Bragg equation:

$$\lambda = 2d_{112} \sin\theta_{112} \qquad (1)$$

Reference lattice parameters (i.e. values for d_0) were also determined in this way from measurements made on the stress-free samples (or combs), and the resulting values were used to generate a two-dimensional map of d_0 in the plane of measurement. It was noted that the values for d_0 were significantly higher in the weld metal for each specimen, and this was attributed to the fusion zone having a different composition to that of the parent plate, noting that these differences in d_0 were not found to vary with the measurement orientation.

For each measurement that was made on a welded plate, the corresponding strain, ε_{112}, was calculated from the measured lattice parameters using:

$$\varepsilon_{112} = \left(d_{112} - d^0_{112}\right)/\, d^0_{112} \qquad (2)$$

in which the strain-free lattice parameter, d^0_{112}, was obtained from the corresponding location within the two-dimensional reference lattice parameter map by linear interpolation. The stresses in the axial, transverse and normal directions can be inferred without knowledge of the principal stresses, from:

$$\sigma_{ii} = \frac{E_{112}}{(1+\nu_{112})}\left[\varepsilon_{ii} + \frac{\nu_{112}}{(1-2\nu_{112})}\left(\varepsilon_{11} + \varepsilon_{22} + \varepsilon_{33}\right)\right] \qquad (4)$$

where σ_{ii} is the relevant stress direction (repeated indices not summed) and E_{112} and ν_{112} are the plane specific Young's modulus and Poisson's ratio, respectively. In this work, values of 222 GPa and 0.277 have been used for E_{112} and ν_{112}, respectively, following Hauk [25].

RESULTS AND DISCUSSION

Satoh Tests

The results of the Satoh tests on the undiluted alloys are shown in Figure 4. In the absence of phase transformations and given the constraint, the tensile stress is expected to increase monotonically as the sample is cooled from 850 ºC, following the respective yield locus. However, at a temperature that corresponds approximately to the expected B_S or M_S temperature there is a reduction in the stress. (Note that the actual B_S/M_S temperature can be affected by the constraining stress.)

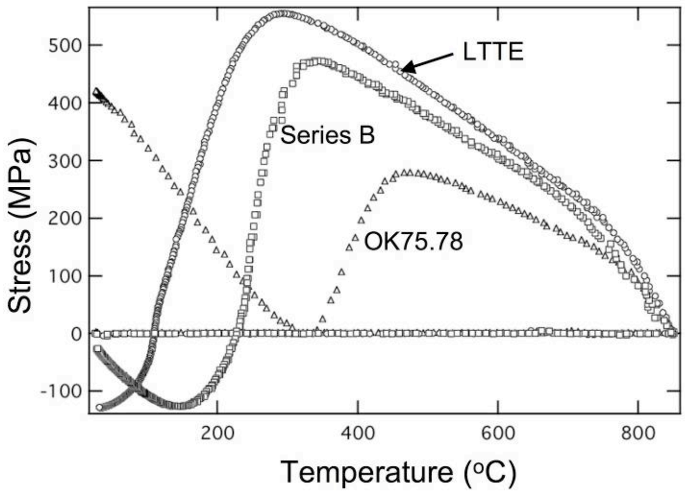

Figure 4: Results of Satoh tests on each of the undiluted weld filler alloys cooling from 850 ºC at 10 ºC s^{-1}.

If the transformation occurs at high temperature, as is the case for OK75.78, significant tensile stress will still build-up once the transformation exhausts. In contrast, the transformation for the LTTE alloy occurs at a sufficiently low temperature for the transformation strain due to the martensitic transformation to completely overwrite the tensile stresses that had accumulated due to thermal contraction, replacing them with compressive residual stresses at ambient temperature. Finally, for Series B, the transformation commences at an intermediate temperature, such that thermal contraction after transformation leaves the constrained test-piece with almost zero stress at ambient temperature.

Stress Measurements on Welded Plates

The longitudinal stresses for each of the welded plates over the mid-length cross section, as mapped by neutron diffraction, are shown in Figure 5. The stress maps are superimposed upon the corresponding macrograph for each weld so that the features of the stress maps can be correlated with the different metallurgical zones. There was a noticeable level of noise in the as-calculated stresses; a symptom of the inherent variability associated with combining three strain measurements and the corresponding stress-free reference measurement needed at each point to infer the stress. This measurement scatter was reduced by averaging the measurements on either side of each weld. In other words, symmetry was assumed about the weld centerline (this was supported by the point-to-point measurements). The processing of the data and the generation of the contour maps were then performed using the Igor Pro analytical software.

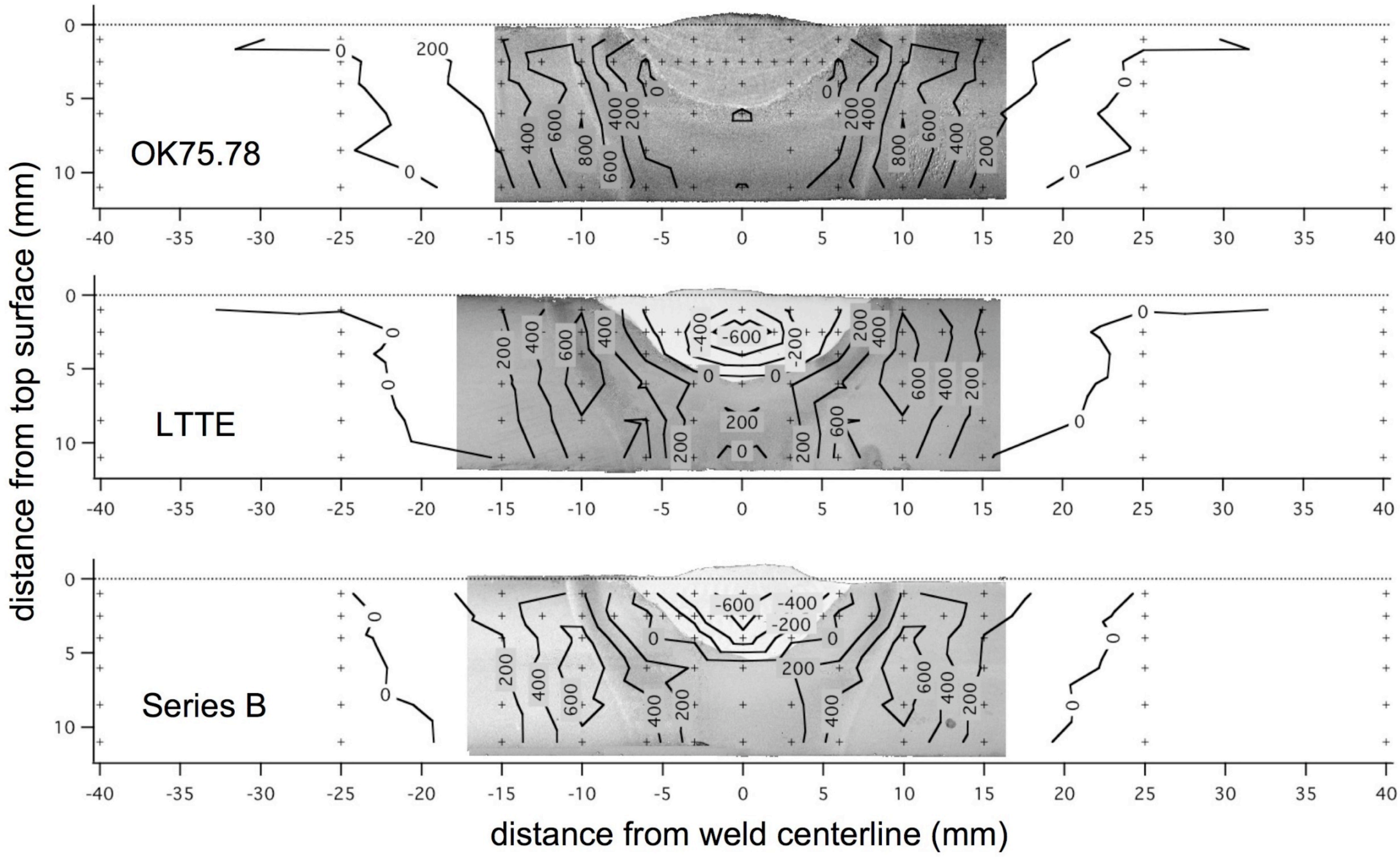

Figure 5: Longitudinal residual stresses across the central 80 mm of each plate estimated using neutron diffraction measurements located at the crosses. For each weld, the stresses are superimposed on the corresponding macrograph.

In the weld made using OK75.78, both the weld nugget and the underlying reaustenitized HAZ will have transformed at relatively high temperatures. Consequently, the stress contours in the HAZ are almost vertical, as if a full-penetration weld has been deposited. The levels of stress both in the weld nugget and underlying region are low but the tensile stresses increase with distance along the horizontal axis, with peak stresses of about 800 MPa located near the HAZ boundary, immediately outside the region that has been influenced by phase transformations, and at about half the depth. The domain in which the stress is greater than 600 MPa is large having a width of just under 5 mm laterally.

Major differences are evident for the LTTE and Series B samples, both of which have weld metals with low transformation temperatures when compared to the plate material. There are major compressive stresses within the weld nuggets. To a depth of 5 mm, the stress contours closely follow the shape of the nugget, i.e., steeply inclined stress contours. This is in stark contrast to those in OK75.78. The phase change within the nugget also appears to have resulted in a reduction of the tensile stresses within the adjacent HAZ up to the depth of 5 mm. The peak tensile stresses were measured to be lower than in the OK75.78 weld and they appear to arise over a smaller region. In the region beneath the nugget for the LTTE and Series B fillers, the phase change occurs at a higher temperature than for the nugget itself. It is therefore possible for tensile stresses to arise in these regions.

The longitudinal stresses for each weld are compared directly in Figure 6. Here each plot corresponds to a different depth below the top surface of the welded plate. The extent to which compressive stresses are induced in the weld nugget by the low transformation temperature filler metals is evident in the plots corresponding to depths of 1, 2.5 and 4 mm respectively. Note that error bars have been included in this figure, to account for the uncertainties in the positions of fitted diffraction peaks, and the corresponding uncertainties in stress are typically smaller than the symbols used, being of the order of 20-30 MPa.

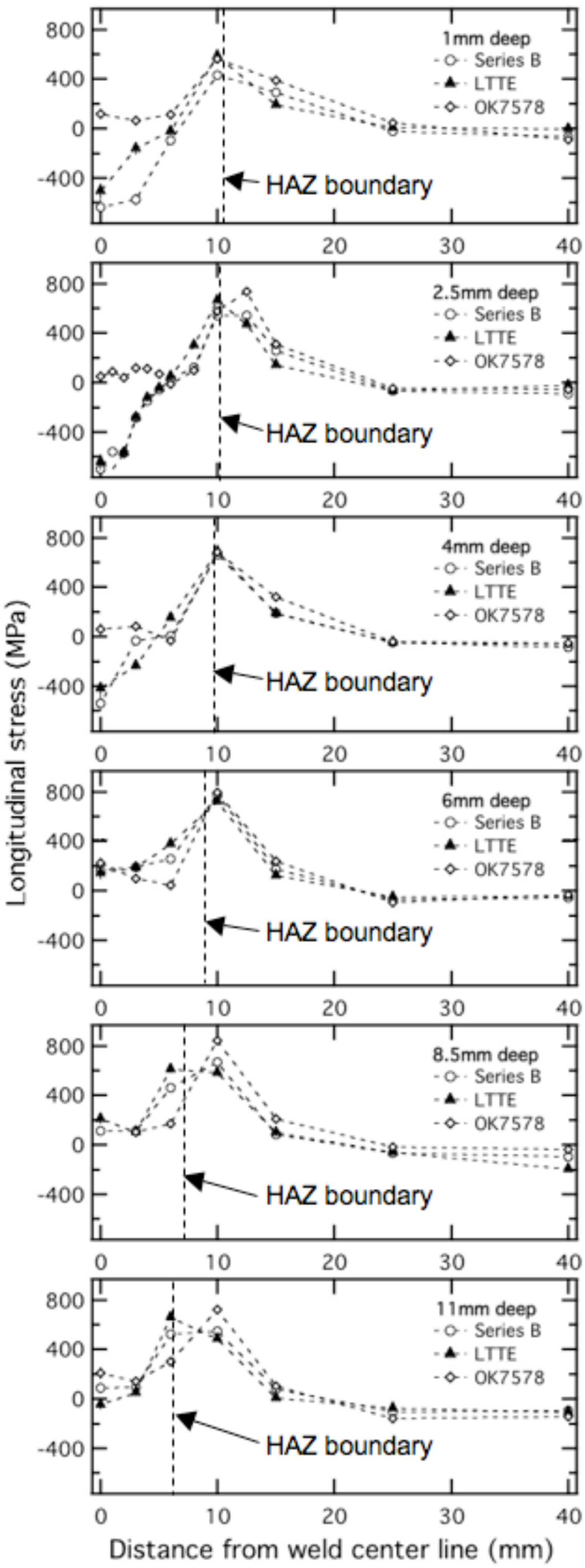

Figure 6: Variation in longitudinal stress with distance from weld centerline at different depths within each welded plate. Note that error bars have been included in this figure that are typically smaller than the symbols used, being of the order of 20-30 MPa. The position of the HAZ boundary, as assessed by optical microscopy, has been highlighted at each depth.

At depths ranging between 6 and 11 mm, the differences between the stress plots are less pronounced. However, it would appear that the peak stresses are generally highest in the weld made with OK75.78. While the tensile regions at these depths are larger in the welds made with LTTE and Series B, the redistribution of stress associated with the low-transformation-temperature fillers appears to have resulted in a slightly lower value for the peak stress. Overall, the highest tensile stresses in the weld made with OK75.78 are found to be just over 800 MPa, whereas the highest stresses in the welds made with both LTTE and Series B are approximately 700 MPa. It would appear, therefore, that while a low-transformation-temperature filler metal can certainly introduce compressive longitudinal stresses to the fusion zone, it may also result in lower peak longitudinal stresses in the weldment as a whole.

The transverse and normal stresses are contrasted for a high transformation temperature (OK75.78) and a low transformation temperature (LTTE) weld filler in Figure 7. The corresponding maps for the Series B alloy are generally similar to those for LTTE. It can be seen that, in the case of the weld made with OK75.78, the transverse stresses are generally very low (<100 MPa) when compared to the longitudinal stress (Figure 5).

In the case of the LTTE weld the transverse stresses through the thickness are approximately parabolic being compressive (~ -300 MPa) near the surfaces and tensile (~ 400 MPa) in the interior. This is presumably caused by the expansion of the nugget after the time at which the HAZ beneath it (and on the centre-line) has already transformed on cooling. In simple terms the nugget essentially acts a bit like a compressive wedge, placing the opposing surface in compression as it causes the HAZ to bend by a small amount elastically. The nature of these stresses fade with increasing lateral distance from the centre-line. Because the nugget and HAZ transform at essentially the same time at the weld centre-line for the OK75.78 weld no bending is introduced in that case. Finite element modelling is currently underway to test this hypothesis.

The normal stresses in the OK75.78 weld are also relatively small when compared to the peaks in longitudinal stress, being less than 200 MPa everywhere. In the case of the LTTE weld, the normal stresses are also generally low, with the largest magnitude corresponding to a zone of compression near to the centre of the weld bead, presumably caused by the volume increase associated with the low temperature transformation. The peak tensile stresses also appear to be less than 200 MPa in magnitude for this component of stress. Of course, the normal stresses must be zero at the top and bottom surfaces of the plates, since these are free surfaces. Such a boundary condition was not imposed when the contour maps were generated, so the fact that the extrapolated normal stresses appear to be low at these surfaces suggests that the stress maps are realistic.

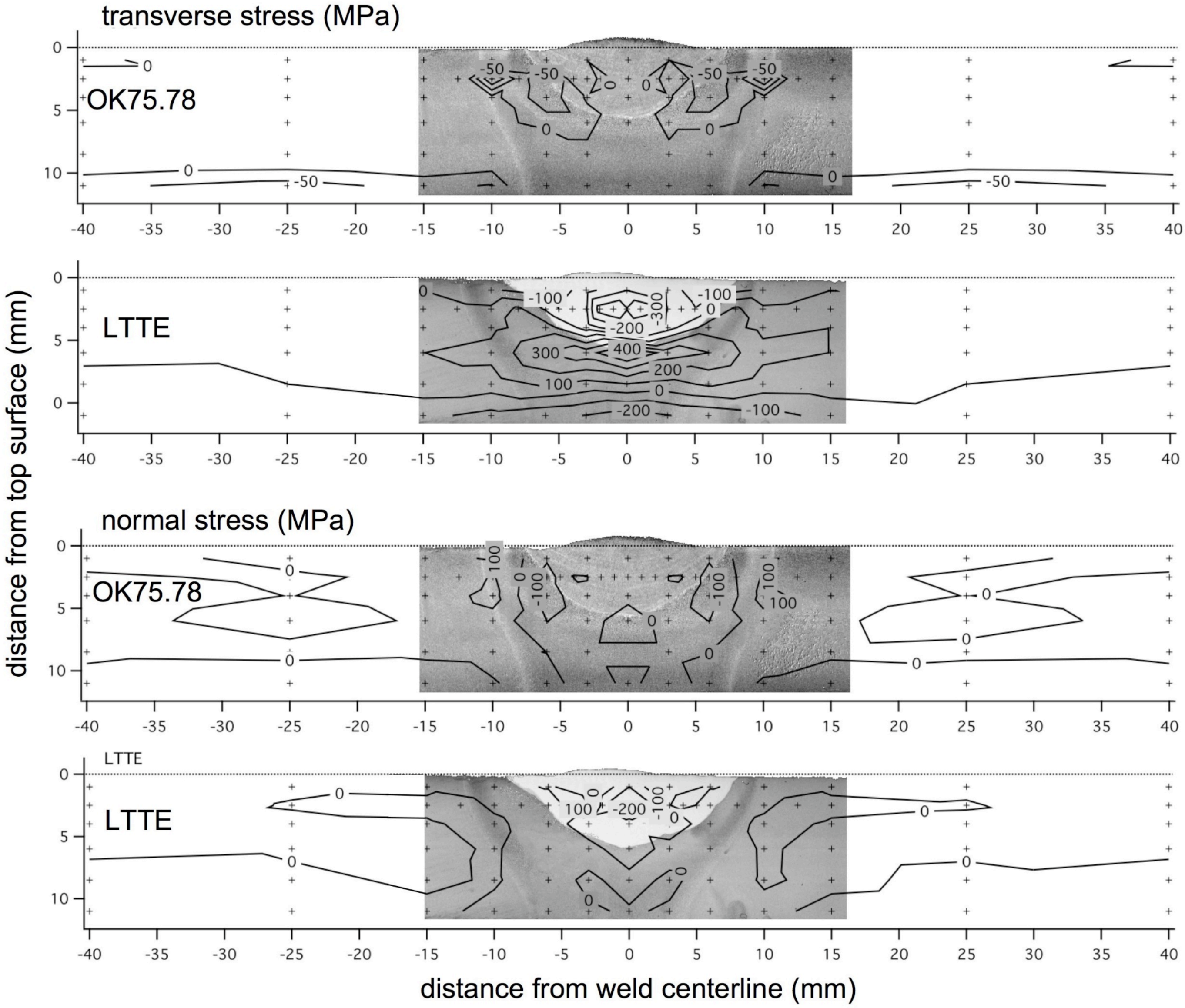

Figure 7: Transverse and normal residual stresses estimated using neutron diffraction measurements at locations marked by crosses for the high transformation temperature OK75.78 filler and the low temperature LTTE filler. The stresses are superimposed on the corresponding macrographs.

Overall, the contour plots for the transverse stress in the LTTE weld raise an interesting philosophical point, in that by generating highly compressive stresses within the weld metal, tensile stresses are introduced elsewhere. In this respect it should be borne in mind that in certain engineering applications the transverse component of stress may be more pertinent to the performance of a component than the longitudinal component of stress. Thus it may be that, in order to achieve optimum stress distributions across a welded joint, it is necessary to optimize the transformation temperature of the filler metal giving consideration to all three components of stress and indeed the difference between the transformation temperature of the filler metal and that of the parent steel.

In summary, when the residual stresses for all three welds are examined, it is evident that the LTTE and Series B alloys have introduced highly compressive longitudinal stresses to the fusion zone and, to a lesser extent, have reduced the peak tensile stresses for the weld configuration as a whole. The highest tensile stresses arose in the longitudinal orientation for all of the welds that were studied, and they resided near the HAZ boundary, immediately outside those regions that had either fully or partially transformed during welding. While the benefits associated with low-transformation-temperature filler alloys are clearly evident in the single-pass groove welds investigated in this study, it is also possible that the observed compensation would have been greater and more uniform if full penetration welds had been made. The potential for mitigation of welding residual stresses in multipass welds using low-transformation temperature filler metals thus offers exciting opportunities for future work.

CONCLUSIONS AND FUTURE WORK

The following conclusions can be drawn for the case of a single weld pass in a Vee-groove on a 12 mm thick bainitic-martensitic steel plate;

- In all three welds solid-state phase transformations have reduced the magnitude and extent of the tensile longitudinal residual stresses that would otherwise be expected in and around the fusion zone relative to welds in which transformations do not take place, being essentially zero in the OK75.78 weld and compressive in welds made with the lower transformation temperature filler metals.
- The peak tensile stresses for each weld were found to arise near the HAZ boundary, immediately outside those regions that had either fully or partially transformed during welding.
- The low-transformation-temperature filler metals resulted in modest reductions in the peak longitudinal tensile residual stresses for the weld configuration as a whole.
- Phase transformations can have large effects on residual stress distributions, and models for welding residual stress development in steels that undergo transformations will need to account for these effects.
- It appears that there is scope to optimize the transformation temperature of a filler metal by giving consideration to all three components of residual stress and the difference between the transformation temperature of the filler metal and that of the parent steel. Indeed, the optimum stress distribution may also depend on the mode of loading and the predominant degradation mechanisms.
- Further work is required to understand how the selection of a low-transformation-temperature filler metal may provide benefits in multi-pass welds where, for many weld passes, the HAZ will reside in previously deposited weld metal.

ACKNOWLEDGMENTS

The authors would like to acknowledge the Worshipful Company of Ironmongers for financial support to help with travel to Canada. HJS would like to thank the EPSRC for the provision of funding, while JAF would like to acknowledge support from Rolls-Royce Naval Marine.

REFERENCES

[1] H.K.D.H. Bhadeshia: “Developments in Martensitic and Bainitic Steels – Role of the Shape Deformation”, *Mat. Sci. Eng. A*, **378**, 34-39, 2004.

[2] P.J. Withers and H.K.D.H. Bhadeshia: “Overview – Residual Stress Part 1 – Measurement Techniques”, *Mat. Sci. Tech.*, **17** (4), 355-365, 2001.

[3] P.J. Withers and H.K.D.H. Bhadeshia: “Overview – Residual Stress Part 2 – Nature and Origins”, *Mat. Sci. Tech,* **17**, 366-375, 2001.

[4] J.A. Francis, H.K.D.H. Bhadeshia, P.J. Withers: “Welding Residual Stresses in Ferritic Power Plant Steels”, *Mat. Sci. Tech*, **23**, 1009-1020, 2007.

[5] A. Ohta, N. Suzuki, Y. Maeda, K. Hiraoka, T. Nakamura: “Superior Fatigue Crack Growth Properties in Newly Developed Weld Metal”, *I. J. of Fatigue*, **21**, S113-S118, 1999.

[6] A. Ohta, K. Matsuoka, N.T. Nguyen, Y. Maeda, N. Suzuki: “Fatigue Strength Improvement of Lap Joints of Thin Steel Plate Using Low-Transformation-Temperature Welding Wire”, *Welding Journal*, **82**, 78S-83S, 2003.

[7] W.X. Wang, L.X. Huo, Y.F. Zhang, D.P Wang, H.Y. Jing: “New Developed Welding Electrode for Improving the Fatigue Strength of Welded Joints”, *J. Mat. Sci. Tech*, **18**, 527-531, 2002.

[8] M. Lord, Ph.D. Thesis, Univ. of Cambridge, 1998.

[9] www.msm.cam.ac.uk/map/steel/programs/MTTT DATA.html#down

[10] H.K.D.H. Bhadeshia: “A Rationalisation of Shear Transformations in Steels”, *Acta Metallurgica*, **29**, 1117-1130, 1981.

[11] H.K.D.H. Bhadeshia: "Thermodynamic Analysis of Isothermal Transformation Diagrams", *Metal Science*, **16**, 159-165, 1982.

[12] S. M. Hodson: "MTDATA-Metallurgical and Thermochemical Databank", *National Physical Laboratory*, Teddington, UK, 1989.

[13] H.K.D.H. Bhadeshia: "Some Phase Transformations in Steels", *Mat. Sci. Tech.*, **15**, 22-29, 1999.

[14] H.K.D.H. Bhadeshia: "The Driving Force for Martensitic Transformation in Steels", *Metal Science*, **15**, 175-177, 1981.

[15] S. Tornblom: "Undermatching Butt Welds in High Strength Steel", Master's Thesis, Lulea University of Technology, ISSN: 1402-1617, Sweden, pp. 60, 2007.

[16] P. Nevasmaa: "Predictive Model for the Prevention of Weld Metal Hydrogen Cracking in High-Strength Multipass Welds", Academic Dissertation, University of Oulu, Finland, *Oulu University Press*, ISBN: 951-42-7180-7, pp. 122, 2003.

[17] Unpublished work: ESAB AB, Central Research Laboratories, Gothenburg, Sweden.

[18] K. Satoh: "Transient Thermal Stresses of Weld Heat-Affected Zone by Both-Ends-Fixed Bar Analogy", *Trans. of the Japan Welding Soc.*, **3**, 125-134, 1972.

[19] K. Satoh: "Thermal Stresses Developed in High-Strength Steels Subjected to Thermal Cycles Simulating Weld Heat-Affected Zone", *Transactions of the Japan Welding Society*, **3**, 135-142, 1972.

[20] J.A. Francis, H.J. Stone, S. Kundu, R.B. Rogge, H.K.D.H. Bhadeshia, P.J. Withers and L. Karlsson: "Transformation Temperatures and Welding Residual Stresses in Ferritic Steels", Paper 26544, Proceedings of the ASME Pressure Vessels and Piping Division Conference (PVP2007), San Antonio, Texas, U.S.A., July 22-26, 2007.

[21] H.J. Stone, P.J. Withers, T.M. Holden, S.M. Roberts, R.C. Reed: "Comparison of Three Different Techniques for Measuring Residual Stresses in an Electron Beam-Welded Plate of Waspaloy", *Metall. Mat. Trans. A*, **30**, 1797-1808, 1999.

[22] M.T. Hutchings, P.J. Withers, T.M. Holden and T. Lorentzen: "Introduction to the Characterisation of Residual Stresses by Neutron Diffraction", *Taylor & Francis*, Boca Raton, Florida, 2005.

[23] P.J. Withers, M. Preuss, A. Steuwer and J.W.L. Pang: "Methods for Obtaining the Strain-Free Lattice Parameter When Using Diffraction to Determine Residual Stress", *Journal of Applied Crystallography*, **40**, 891-904, 2007.

[24] H.K.D.H. Bhadeshia and R.W.K. Honeycombe: "Steels – Microstructure and Properties", 3rd edn., *Butterworth-Heinemann*, Oxford, pp. 287-306, 2006.

[25] V. Hauk: "Structural and Residual Stress Analysis by Nondestructive Methods", *Elsevier Science B.V.*, ISBN 0 444 82476 6, 1997.